The properties of polycyclic aromatic hydrocarbons in galaxies: constraints on PAH sizes, charge and radiation fields

D. Rigopoulou,[1]★ M. Barale,[1,2] D. C. Clary,[3] X. Shan,[3] A. Alonso-Herrero,[4] I. García-Bernete,[1]
L. Hunt [ID],[5] B. Kerkeni,[1,6,7] M. Pereira-Santaella [ID][1,8] and P. F. Roche[1]

[1]*Astrophysics, Department of Physics, University of Oxford, Keble Road, Oxford OX1 3RH, UK*
[2]*Université de Rennes, CNRS, ISCR (Institut des Sciences Chimiques de Rennes), UMR 6226, F-35000 Rennes, France*
[3]*Physical & Theoretical Chemistry Laboratory, University of Oxford, South Parks Road, Oxford OX1 3QZ, UK*
[4]*Centro de Astrobiología, CSIC-INTA, ESAC Campus, E-28692, Villanueva de la Cañada, Madrid, Spain*
[5]*INAF, Osservatorio Astrofisico di Arcetri, Largo E Fermi 5, 50125 Firenze, Italy*
[6]*Département de Physique, LPMC Faculté des Sciences de Tunis, Université de Tunis el Manar, Tunis 2092, Tunisia*
[7]*ISAMM, Université de La Manouba, La Manouba 2010, Tunisia*
[8]*Centro de Astrobiología (CSIC-INTA), Ctra. de Ajalvir, km 4, E-28850 Torrejón de Ardoz, Madrid, Spain*

ABSTRACT

Based on theoretical spectra computed using Density Functional Theory we study the properties of polycyclic aromatic hydrocarbons (PAH). In particular using bin-average spectra of PAH molecules with varying number of carbons we investigate how the intensity of the mid-infrared emission bands, 3.3, 6.2, 7.7, and 11.3 μm, respond to changes in the number of carbons, charge of the molecule, and the hardness of the radiation field that impinges the molecule. We confirm that the 6.2/7.7 band ratio is a good predictor for the size of the PAH molecule (based on the number of carbons present). We also investigate the efficacy of the 11.3/3.3 ratio to trace the size of PAH molecules and note the dependence of this ratio on the hardness of the radiation field. While the ratio can potentially also be used to trace PAH molecular size, a better understanding of the impact of the underlying radiation field on the 3.3 μm feature and the effect of the extinction on the ratio should be evaluated. The newly developed diagnostics are compared to band ratios measured in a variety of galaxies observed with the Infrared Spectrograph on board the *Spitzer Space Telescope*. We demonstrate that the band ratios can be used to probe the conditions of the *interstellar medium* in galaxies and differentiate between environments encountered in normal star forming galaxies and active galactic nuclei. Our work highlights the immense potential that PAH observations with the *James Webb Space Telescope* will have on our understanding of the PAH emission itself and of the physical conditions in galaxies near and far.

Key words: methods: data analysis – ISM: molecules – galaxies: ISM – galaxies: star formation – infrared: ISM.

1 INTRODUCTION

Strong emission features at 3.3, 6.2, 7.7, 8.6, 11.3, and 12.7 μm are commonly attributed to mixtures of polycyclic aromatic hydrocarbons (PAHs) that are large molecules resulting from fusion of aromatic rings and related species (Tielens 2008). Upon absorption of ultraviolet (UV) photons, PAH molecules become highly vibrationally excited and subsequently relax through emission of infrared (IR) photons at specific wavelengths (Draine & Li 2007). The absorption efficiency of PAHs has been modeled based on astrophysical observations, laboratory measurements, and quantum theory (e.g. Joblin, Leger & Martin 1992; Draine & Li 2001, 2007; Verstraete et al. 2001; Malloci, Joblin & Mulas 2007). In addition to being major radiative coolants of the Interstellar medium (ISM), PAHs are also responsible for most of the photoelectric heating of the gas in photodissociation regions (PDRs) and the neutral ISM, due to their high cumulative surface area (Bakes & Tielenss 1994;

Hollenbach & Tielens 1997). As such, PAHs play an important role in the energy balance of the ISM.

The ubiquity of these mid-infrared (mid-IR) features in a wide variety of astrophysical objects and enrivonments provides a useful diagnostic of the physical conditions in these sources. Mid-IR spectroscopic observations with *ESA's Infrared Space Observatory* (Kessler et al. 1996) and NASA's *Spitzer Space Telescope* (Werner et al. 2004) of a number of galactic and extragalactic sources have confirmed that PAH features are found to dominate the spectra of evolved stars (Blommaert et al. 2005) all the way to spectra of entire galaxies (Brandl et al. 2006; Smith et al. 2007). From an extragalactic point of view, the strengths of the 7.7 and 6.2 μm features have been proposed as tracers of star formation (e.g. Rigopoulou et al. 1999; Peeters, Spoon & Tielens 2004). The diagnostic power of these features to trace star formation has been thoroughly investigated (e.g. Shipley et al. 2016) and applied out to the highest redshift sources (e.g. Huang et al. 2007; Pope et al. 2013; Riechers et al. 2014). However, there are claims that the tracers are affected by global galaxy parameters such as the metallicity (Engelbracht et al. 2008; Hunt et al. 2010).

The picture becomes more complicated for galaxies that host an active galactic nucleus (AGN). Galaxies with AGN tend to have low 6.2 and 11.3 μm PAH equivalent width (e.g. Roche, Aitken & Smith 1989; Rigopoulou et al. 1999; Tran et al. 2001; Sturm et al. 2000; Desai et al. 2007; Diamond-Stanic & Rieke 2010) due to the presence of a significant hot dust continuum and also because the hard AGN photons may destroy the small PAH molecules. However, more recent ground-based observations detect the 11.3 μm PAH feature at distances of hundreds to tens of parsecs from the AGN (e.g. Hönig et al. 2010; González-Martín et al. 2013; Alonso-Herrero et al. 2014, 2016). Moreover, there are indications that the AGN may also be the source of PAH excitation (Jensen et al. 2017). A recent review by Li (2020) highlights our current understanding of the impact of specific galaxy properties on the strength of the PAH bands.

The detailed characteristics of PAHs, such as their central wavelength, shape, and the intensity ratio between different bands, are known to vary (Peeters et al. 2004). These variations primarily reflect changes in the structure of the PAH molecules in response to diverse astrophysical environments. Because each PAH band is attributed to a specific vibrational mode, the ratio between different bands could be used as a diagnostic of PAH properties. For instance, it is well known that the 3.3 μm PAH feature is due to the radiative relaxation of C–H stretching modes, the 6–9 μm features originate from C–C stretching modes while the 11.3 μm feature originates in the C–H out-of-plane bending modes. Experimentally, it has also been confirmed that the C–C modes are intrinsically weak in neutral PAHs compared to ionized PAHs (Allamandola, Hudgins & Sandford 1999; Bauschlicher 2002; Kim & Saykally 2002). Therefore, the 6–9 μm features will be much more prominent for ionized PAHs, while the converse is true for the 3.3 and 11.3 μm bands. Consequently, the ratios between the C–C and the C–H feature intensities depend on the charge of the PAHs, which is directly related to the physical conditions in the environment where the emission is originating.

A number of authors have presented evidence for the existence of variations between the strength of PAH bands in different astrophysical environments but also within a given source (Hony et al. 2001; Galliano et al. 2008; Peeters et al. 2017). Bregman & Temi (2005) studied the variation of the 7.7/11.3 ratio in reflection nebulae and found a correlation of this band ratio with the ratio G_0/n_e between the integrated intensity of the UV field, G_0, and the electron density, n_e. However, Smith et al. (2007) concluded that this ratio is relatively constant among pure starburst galaxies but varies by a factor of 5 among galaxies having a weak AGN. They interpret this effect as a selective destruction of the smallest PAHs by the hard radiation arising from the accretion disk, ruling out an explanation in terms of ionization of the molecules, in these particular environments.

The use of PAH band ratios as diagnostics of the physical conditions of the ISM has been established in previous works (e.g. Hony et al. 2001; Sloan 2007; Galliano et al. 2008; Stock & Peeters 2017). In this paper we use theoretically computed PAH spectra to investigate how the PAH molecular size (in this work parameterized by the number of carbons N_c), the PAH charge (ionized versus neutral), and the average photon energy affect the relative intensities of each PAH band. The aim of this work is to assess through our analysis the use of PAH band ratios as diagnostics of the physical conditions of the ISM in galaxies. In particular we wish to investigate how the measured PAH band ratios can be used to infer PAH molecular sizes, charge, and the hardness of the radiation field that excites the PAHs. As we are using PAH band ratios measured in relatively large regions (∼kpc scale) in galaxies (using spectra from *ISO* and Spitzer) the focus of this work is not to *identify specific*

PAH or even classes of PAH molecules but instead to carry out a qualitative investigation of the PAH band ratios.

The paper is arranged as follows. In Section 2 we discuss the theoretical approach and the methodology followed to compute PAH theoretical spectra using Density Functional Theory (DFT) as well as the emission model used. A detailed description of the molecules included in this work is also presented. In Section 3 we present the model PAH spectra and measure the intensities of the various features. Sections 4 and 5 contain the results and discussion of their astrophysical implications followed by conclusions which are summarized in Section 6.

2 METHODOLOGY

When an interstellar PAH molecule absorbs a UV photon the energy is quickly transferred to the vibrational levels and the molecule proceeds to an excited state. Once excited, the molecule will cool by fluorescence and emit IR photons at the frequencies that correspond to specific vibrational modes (Allamandola et al. 1999; Bakes & Tielenss 1994). It has been shown (Allamandola, Tielens & Baker 1989) that the IR fluorescence of such molecular sized species is well approximated by the product of the absorption cross section convolved with the *Planck* function as was proposed by Leger & Puget (1984). This approach has formed the cornerstone of most theoretical modeling studies of interstellar PAHs. Since some vibrational modes (in particular stretching of C–C and bending of C–H bonds) are common to most PAHs and also occur at similar frequencies, a significant population of PAHs will emit very strongly at those common frequencies. As a consequence, the observed emission bands are overall fairly similar in appearance in different lines of sight.

The intrinsic spectral characteristics of PAHs, such as their vibrational frequencies, can be computed with a variety of techniques summarized in Tielens (2008). The focus of these methods is to solve Schrödinger's equation for molecular systems with many electrons using a specific set of approximations. All of the theoretical PAH spectra used in this work have been computed using DFT. The method provides a cost-effective approximate solution of Schrödinger's equation and has made very useful predictions of spectra of PAHs that compare favourably with available experimental data (Tielens 2008).

2.1 Selection criteria

A large number of DFT calculations of PAH vibrational frequencies have been reported in the literature. The molecules used in the present study are built with the GAUSSVIEW 5 software and the DFT calculation were performed using Gaussian 09 (Frisch et al. 2009) together with the B3LYP functional along with the 4-31G basis set. The functional enables the optimization of the molecular structure while the basis set provides the mathematical functions that describe the molecular orbitals. These are expressed as linear combinations of the basis whose size controls the accuracy of the solution and the computational cost. A detailed discussion of the various methods used to compute PAH vibrational frequencies and their characteristics is included in a forthcoming paper (Kerkeni et al., in preparation). Harmonic frequencies and IR intensities have been computed for large solo-containing neutral and cationic forms of PAH molecules. For the present study we have also used spectra from the NASA Ames PAH IR Spectroscopic Database (Boersma et al. 2014; Bauschlicher, Ricca & Boersma 2018; Mattioda et al. 2020). The study includes PAH molecules based on the following criteria:

(1) Number of carbons $20 < N_c < 400$

(2) Availability of neutral and singly cationic spectra

(3) Absence of O, N, Fe, Mg in the molecules

The entire sample used in this study is listed in Appendix A.

2.2 Assumptions and emission model parameters

The DFT-computed transition frequencies must be convolved with a specific band shape, line width, and emission temperature to convert them into an emission spectrum similar to those observed in astrophysical environments. In what follows we briefly discuss how the DFT results for frequencies and intensities can be converted into synthetic models for the PAH emission occurring in astrophysical environments.

2.2.1 Band profiles and band shifts

While profiles from single vibrational transitions show a Lorentzian shape, the observed bands result from a superposition of Lorentzians of slightly different peaks and widths. This happens because of the emission process and of the different temperatures that each PAH attains upon absorption of a photon. Observationally, PAHs have been fit by Drude profiles (Smith et al. 2007) as well as Lorentzian ones and Peeters et al. (2017) discussed the issue in more detail. For the present study we have adopted Lorentzian profiles for each PAH transition. The adopted profiles can be parameterized as

$$\Pi(\nu) = \frac{1/2\Gamma}{\pi(\nu - \nu_i)^2 + (1/2\Gamma)^2}, \qquad (1)$$

where Γ (cm^{-1}) is the full width at half-maximum (FWHM) of the feature and ν_i is the frequency of the mode i. The FWHM of the profiles observed in astronomical objects are found to vary substantially amongst the different wavelength regions. Peeters et al. (2004) found that the mid-IR PAH features show line widths of 10–30 cm^{-1} while for the longer wavelength bands (beyond 15 μm) the features are typically 4–8 cm^{-1} (Moutou et al. 1998). Since in this work we focus on the 2.5–15 μm region we adopt a FWHM value of 30 cm^{-1} for all the features.

The vibrational frequencies are computed using the harmonic approximation. To account for limitations in theory and also for anharmonic corrections and to ensure a better agreement with experimental spectra the frequencies *need to be scaled* appropriately. Typically, *a scaling factor* of 0.958 for B3LYP/4–31G is used for simplicity for the entire spectrum, based on comparison with matrix-isolation data. However, it is known that this technique may introduce unpredictable shifts in the band positions (Langhoff et al. 1994). For the spectra used here we have applied a wavelength-specific scaling factor as follows: 0.956 for wavelengths less than 2 μm, 0.952 for wavelengths between 4 and 9 μm and 0.96 for wavelengths beyond 9 μm.

2.2.2 Emission model & band intensities

Relative emission band intensities depend on the excitation energy (temperature) that the PAH attains and must be taken into account when considering the mid-IR emission spectrum. Several approaches exist (e.g. Allamandola et al. 1989) the simplest approximation amounts to multiplying the intensity in each band with the *Planck* function at a specific emission temperature:

$$B(\nu_i, T) = \frac{2hc\nu_i^3}{exp(\frac{hc\nu_i}{k_B T}) - 1}, \qquad (2)$$

where ν_i (cm^{-1}) is the frequency of the transition i, T (K) is the average emission temperature, h (erg s) is *Planck*'s constant, c (cm s^{-1}) is the speed of light, and k (in erg K^{-1}) is Boltzmann's constant. In reality however, the temperature that each PAH molecule will attain upon absorption of a photon depends on a number of parameters including the energy of the absorbed photon, the heat capacity (C_V), and the photo-absorption cross section (σ_i) of the given PAH.

Leger, d'Hendecourt & Defourneau (1989) proposed that the IR cooling of PAHs can be described with the thermal approximation. In this case the PAH molecule can be considered as a heat bath with an average molecular energy U and temperature T. Following absorption of a UV photon, the molecule has an internal energy U(T) which can be written as

$$U(T) = \sum_i^n \frac{hc\nu_i}{exp(hc\nu_i/k_B T) - 1}. \qquad (3)$$

Upon absorption of a photon with energy hcν, the PAH will attain a peak temperature T_p according to

$$C_V(T)dT = hc\nu, \qquad (4)$$

where $C_V(T)$ is the heat capacity of the PAH molecule that is related to its internal energy via

$$\int_{2.73}^{T_p} C_V(T)dT \equiv dU(T)/DT, \qquad (5)$$

where 2.73 is the cosmic microwave background temperature. Once the molecule has attained its peak temperature it will cool via its various vibrational modes, through a so-called radiative cascade. The fractional energy emitted in a given mode corresponds to a fall in internal energy δU

$$\delta E_i \propto \delta U(T). \qquad (6)$$

The total energy emitted in a single band is obtained by integrating over the temperature range from 2.73 K to the peak temperature (T_p), weighted by the rate of photon absorption given by

$$\sigma_i = \int_{2.73}^{T_p} \frac{B_{\nu,i}^T \sigma_{\nu,i}}{h\nu} d\nu, \qquad (7)$$

where ν is the frequency of the absorbed photon, σ_ν is the frequency-dependent photoabsorption cross-section, $B_{\nu,i}^T$ is the *Planck* function at frequency ν, and temperature T and T_{max} represents the high-energy cut-off in the radiation field. For each molecule, σ_ν was taken from Draine & Li (2001) and Mattioda et al. (2005).

Under this model each PAH molecule reaches a different maximum temperature that depends on its heat capacity, with the subsequent radiative relaxation from that excitation level or temperature taken into account. The emission model makes use of the thermal approximation discussed in Verstraete et al. (2001).

Clearly, a modification of the temperature distribution of the PAHs will affect the relative strength of the emission features. One way to change the PAH temperature is by changing the energy of the UV photons that are absorbed by PAHs. In an astrophysical setting this would correspond to e.g. a change in the spectral hardness of the underlying radiation field. Habing (1968) introduced the dimensionless parameter

$$\chi = \frac{\nu u_\nu}{4 \times 10^{-14} \text{erg cm}^{-3}}, \qquad (8)$$
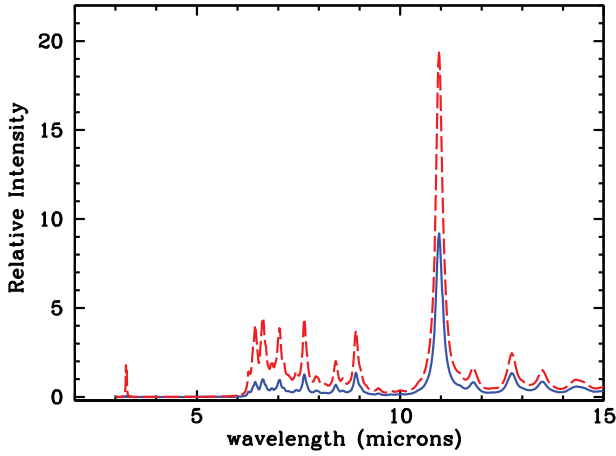
Figure 1. Comparison of the emission features of a PAH molecule with N_C = 210 that is exposed to a radiation field of 5 eV (blue line) and 12 eV (red dashed line). The *y*-axis represents the normalized intensities of the features.
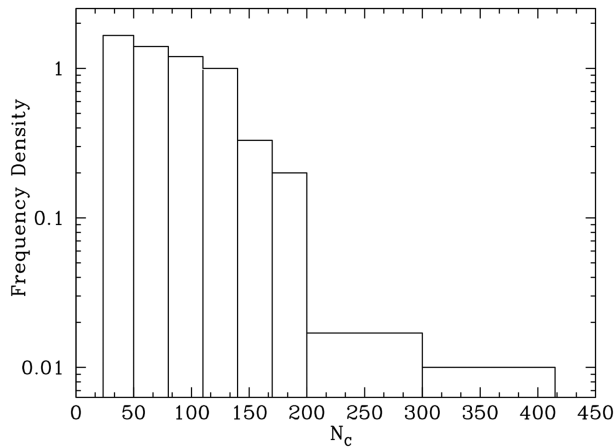
Figure 2. Histogram depicting the intrinsic size distribution of all neutral PAH molecules in this study. Species have been placed into bins of unequal width size as discussed in the text.

and determined that $\nu u_\nu \sim 4 \times 10^{-14}$ erg cm^{-3} at λ = 1000 Å, corresponding to an average photon energy of $\sim$12.4 eV for the interstellar radiation field (ISRF) in the solar neighbourhood. We have used the emission model outlined above to generate PAH spectra corresponding to (absorbed) photons at various energies. In Fig. 1 we show an example of the resulting PAH spectra corresponding to a neutral large PAH molecule (with N_C = 210 carbon atoms) when it absorbs a photon of 5 eV (blue line) and one of a 12.4 eV (red dashed line). As is evident from Fig. 1 the peak intensity of each emission feature varies depending on the energy of the photon that was absorbed. For example, the peak intensity of the 3.3 μm feature varies by a factor of ($I_{3.3(12.4eV)}/I_{3.3(5eV)}$) $\sim$11, that of the 11.3 μm feature varies by a factor of ($I_{11.3(12.4eV)}/I_{11.3(5eV)}$) $\sim$2 while the ratio of the intensities of the 6.2 and 7.7 μm features is less sensitive to changes in the photon energy.

3 THE PAH SPECTRA

Determining the nature, composition, and exact make-up of the emitting PAH population in astronomical objects is far from trivial. While spectral decomposition has been demonstrated as a promising tool for identifying classes of PAHs in galactic sources (e.g. Boersma, Bregman & Allamandola 2013; Bauschlicher et al. 2018) this method is not suitable for galaxies given that the beam-averaged emission encompasses a wide range of PAH molecules of varying size, charge, and composition. In this work we adopt a slightly different approach: by examining the theoretically computed PAH IR spectra of different size, geometry, charge, and emission model, our aim is to determine how the different PAH emission bands change as we step through changes in the properties of the PAH molecules. For the work presented here the focus is not on identifying specific species but establishing how the properties of PAH molecules influence the strength of each of the most prominent emission bands and how external conditions such as the strength of the radiation field to which a PAH molecule may be exposed affects the strength of these bands. For this purpose, we have ensured that, all the DFT spectra used in the analysis show broadly the characteristics that dominate the observed mid-IR spectra of galaxies, namely, the presence of a wide underlying plateau in the 6–9 μm and the strong 11.3 μm PAH expected to arise mainly from large neutral molecules.

A histogram of the distribution of all PAH molecules used in this work, as a function of size (parameterized by the number of carbons N_C), is shown in Fig. 2. Since more PAH molecules with N_C < 150 are available in our PAH sample (compared to larger molecules) the bins in the histogram have unequal widths. Because of that the vertical axis encodes the frequency density per unit bin size, which is defined as the ratio of frequency over width for each bin (Venables & Ripley 2002). The plot illustrates that the number of large PAH molecules drops significantly beyond N$_C$ >200 and we discuss this issue further in Section 5.

The computed spectra were all processed following the steps outlined in Section 2. The emission model discussed in Section 2 was applied whereby the PAHs are excited upon absorption of photons of a certain energy. In the present work we considered emission models corresponding to photons of a range of energies from ISRF to 10^3 × ISRF. We then measured the 3.3, 6.2, 7.7, 8.6, and 11.3 μm emission band intensities for all the PAH spectra. The emission band intensities were measured using the publicly available software CASSIS[1] (Vastel et al., 2015) in much the same way that we measure observed spectra from astronomical sources.

Astronomical mid-IR PAH features are found on top of broad underlying plateaus that represent continuum emission from small grains heated by stellar light. Different methods have been used to separate PAH features from the underlying warm dust continuum either by fitting a spline through fixed points (Peeters et al. 2004) or by fitting Drude profiles (e.g. PAHFIT, Smith et al. 2007) or Lorenztian profiles (Boulanger et al. 1998). However, as Galliano et al. (2008) pointed out although different methods lead to different implied band intensities, PAH intensity band ratios should be largely insensitive to the specific method. For the present study we treat the DFT spectra as 'real' astronomical spectra. We use a first order polynomial to account for the underlying continuum. We then identify the wavelength at which each feature peaks and use this as a first guess for the line fits. A Lorentzian function is then fit to each PAH emission feature which is centred at the wavelength identified for each feature. The width and height of the Lorentzian were left as free parameters during the fit. Fig. 3 shows an example of the fitting procedure for $C_{54}H_{18}$. Since DFT-computed PAH spectra exhibit shifts in the positions of the main features, depending on

[1] http://cassis.irap.omp.eu
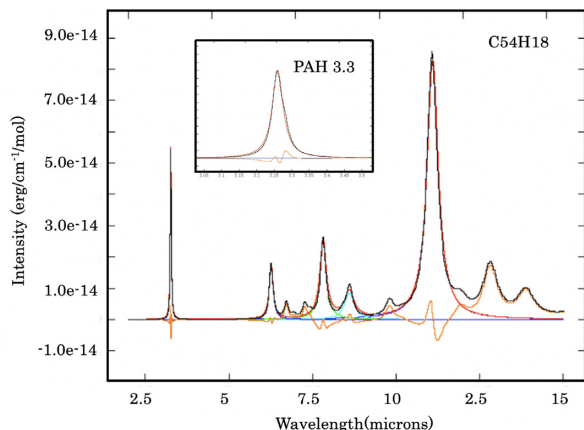
Figure 3. An example of the fitting procedure adopted to measure the intensity of the bands of a DFT-computed PAH spectrum (black line) with $N_C = 54$ ($C_{54}H_{18}$). exposed to the ISRF hardness. Each spectral band is fitted assuming a Lorenzian (corresponding to different colours). The inset figure shows the fit for the 3.3 μm band. The orange line denotes the residuals of the fit. The width, height, and central wavelength are left as free parameters during the fit.

the presence of even/odd carbons (Ricca et al. 2018) as well as the geometry, we do not fix the central wavelength of the features, but rather use it as a first guess for the fit. This is particularly important in the location of the 11.3 μm feature (which is made up of sub-features in the entire 11.0–11.3 μm range). Hence, particular care was taken during the fits so that the integration was done under the appropriate range and for this reason the central wavelength was left as a free parameter during the fits. Our method measures intensities in the DFT-computed spectra in a similar way to that followed for observed spectra, with the caveats outlined above. Our method for measuring band intensities differs from that followed by Maragkoudakis, Peeters & Ricca (2020) where the emission band fluxes are determined by summing over the flux between pre-determined wavelength ranges.

For each of the individual bins shown in Fig. 2 we then calculate a composite PAH spectrum. This was done by averaging the spectra in that bin and that means for every bin (and every PAH feature) we determined the arithmetic mean by dividing the average value by the number of molecules that were assigned to that bin. If for a specific PAH molecule its flux value was found to deviate by more than 3σ from the average value determined for the feature then the spectrum from that PAH molecule was discarded from that bin. Therefore, each bin is represented by the averaged spectrum of all the molecules in that bin.

Fig. 4 shows the relative intensities of the 3.3, 6.2, 7.7, 8.6, 11.3 μm PAH emission bands calculated based on the ISRF emission model (see Fig. B1 for the same plot for cations). The figure shows the average intensities as well as the 3σ spread around this value for every bin. All five emission bands show a dependence on N_C although with noticeable scatter that is more pronounced for bands 6.2 and 7.7 μm. The least scatter appears in the 11.3 μm band which is perhaps not surprising given that neutral PAHs contribute significantly to the emission in the band. The intensity of the 3.3 μm band decreases with increasing number of carbons N_C as expected since the 3.3 μm band is most sensitive to the smallest PAHs (Schutte, Tielens & Allamandola 1993).

4 PAH BAND RATIOS: SIZE, CHARGE, HARDNESS OF THE RADIATION FIELD

The spectral bands and their variations can be used to probe the size, charge, composition, and the underlying radiation field of PAHs. In particular, the size distribution of PAH molecules is important with large molecules contributing more to bands at longer wavelengths whereas smaller PAHs are responsible for the emission at shorter wavelengths (Allamandola et al. 1989).

4.1 Band ratios versus PAH size distribution

We start off by examining the dependency of the various intensity band ratios on the size of the PAH molecules. The 6.2 μm and 7.7 μm bands are attributed to stretching modes of C – C bonds, while the 3.3, 8.6 and 11.3 μm bands are due to the stretching modes, in-plane bending modes, and out-of-plane bending modes of C–H bonds (Allamandola et al. 1989). Hence, the ratios of different PAH bands arising from the same vibrational modes (e.g. 6.2/7.7 and 11.3/3.3) could be used to infer the size distribution of PAHs (Jourdain de Muizon et al. 1990; Sales, Pastoriza & Riffel 2010). A number of studies aimed at determining PAH size distribution in the Spitzer era have relied upon the use of the 6.2 and 7.7 μm features as these are the brightest ionic features in the mid-IR spectra of galactic and extragalactic sources. Draine & Li (2001) introduced the 6.2/7.7 and 11.3/7.7 ratios as indicators of PAH size and ionization, respectively. The Draine & Li (2001) models are based on numerical calculations using realistic estimates of absorption cross sections depending on the number of C atoms, the H/C ratio, and the ionization state of the PAHs. Absorption cross sections have been taken from Allamandola et al. (1999). The Draine & Li (2001) analysis follows the creation of a model PAH grain of a given size that is subsequently exposed to radiation fields of varying strengths followed by calculation of the resulting emission spectrum. Fig. 5 shows the intensity ratio of 6.2/7.7 as a function of N_C for the DFT-computed PAH molecules studied here. Each point in the plot represents the PAH band ratio measured from the averaged spectrum for that bin.

We find that the 6.2/7.7 ratio tracks N_C with the ratio decreasing by a factor of ~2 between small and large values of N_C. We note that Maragkoudakis et al. (2020) found significant scatter in the 6.2/7.7 ratio as a function of N_C and argued against the effectiveness of the ratio to trace PAH size. A number of reasons could be responsible for the different outcomes: First, there are differences in the measured PAH band intensities. Maragkoudakis et al. (2020) measure PAH bands by summing the flux between pre-determined wavelength ranges and apply no separate treatment for the 6–9 μm emission plateau. In the present work (outlined in Section 3), a set of Lorentzians are fit to the PAH emission features. Our methodology follows the profile decomposition method described by Smith et al. (2007) although in the case of the DFT spectra there is obviously no dust continuum emission. In this work each PAH feature is fit by a Lorentzian profile where the width and the central wavelength of the feature are allowed to vary as has been the case for fitting extragalactic PAH spectra from Spitzer and *ISO* (see Smith et al. 2007 and references therein).

While the two approaches result in relative agreement in the fluxes measured for the 'isolated' PAH features such as the 3.3 and the 11.3 μm, there are significant differences in the measured fluxes for the features in the 6–9 μm wavelength regime.

The DFT spectra often show significant (sub-)structure around the 5–9 μm range with the complexity increasing with increasing number of carbons. As e.g. Ricca et al. 2012 point out the number of
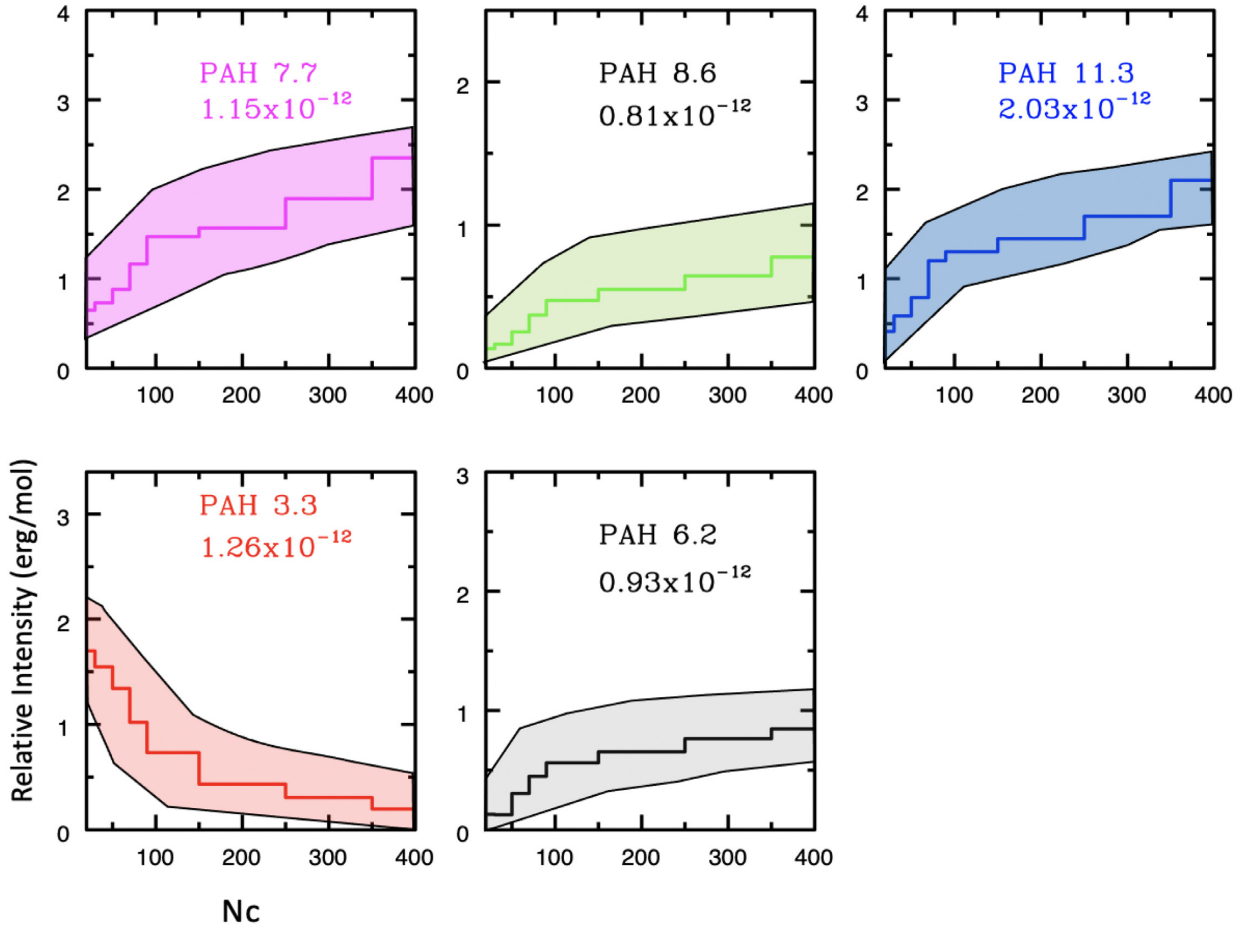
Figure 4. Intensities for neutral PAHs (3.3, 6.2, 7.7, 8.6 and 11.3 μm) as a function of N_C, with normalizations shown in each panel. The average value in each bin is denoted with the line while the shaded regions denote the spread of values in each bin. PAHs with intensity values greater than 3σ have been excluded. The intensities have been calculated for the ISRF radiation field. Colour coding: 3.3 μm (red), 6.2 μm (grey), 7.7 μm (magenta), 8.6 μm (green), 11.3 μm (blue).
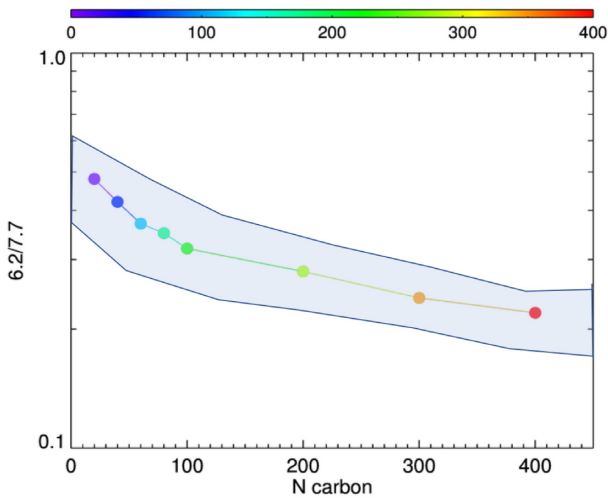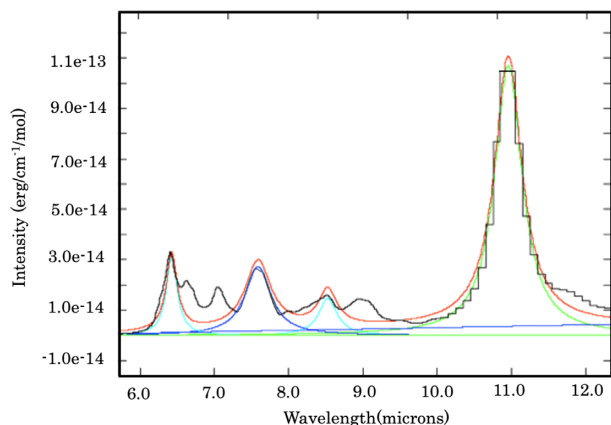

Figure 5. The 6.2/7.7 intensity ratio as a function of N_C for neutral PAHs exposed to the Galaxy ISRF radiation. The shaded region corresponds to the spread of values of each individual PAH considered in this study (see Section 3).

C–C and C–H bonds increases with increasing PAH size. This leads to an increase in the possible ways that the C–C and the C–H modes can couple that subsequently results in an increase in the number of features in the 6–9 μm wavelength regime.

The second, and perhaps, more important reason for the differences is the bin-averaging that we employ in our analysis. Given that the focus of the present work is on PAH spectra from extragalactic sources (and therefore beam averaged spectra of a number of individual PAHs) we have bin-averaged the DFT spectra based on bins of N_C shown in Fig. 2. In addition, for the final averaged spectra in each bin we have excluded those spectra for which the flux in a given PAH band was found to deviate by more than 3σ from the average value determined for that band in that specific bin. Fig. 6 shows the 6–12 μm range of the averaged spectrum in the $100 < N_C < 150$ bin where each PAH feature is fit with a separate Lorentzian centred at the nominal wavelength. Our fits for the 6.2 (cyan) and 7.7 (blue) PAH features result in a ratio of 6.2/7.7 ~0.35 in agreement with the band ratio versus N_c plot shown in Fig. 5.

Next, we consider the 11.3/3.3 ratio as a function of N_C, shown in Fig. 7. As already noted, both the 3.3 and 11.3 μm bands originate from stretching and bending of the C–H bonds therefore their ratio could be suitable to trace PAH molecular size. A number of authors (e.g. Mori et al. 2012; Ricca et al. 2012; Croiset et al. 2016; Maragkoudakis et al. 2020) have used the ratio to trace PAH size distribution. We find that the 11.3/3.3 ratio tracks N_C with the ratio

Figure 6. The 6–12 µm range of the averaged PAH spectrum in the $100 < N_C < 150$ bin. The cyan, blue, and green lines denote the Lorentzian fits to the 6.2, 7.7, and 11.2 µm PAH features (see text for details of the fits).
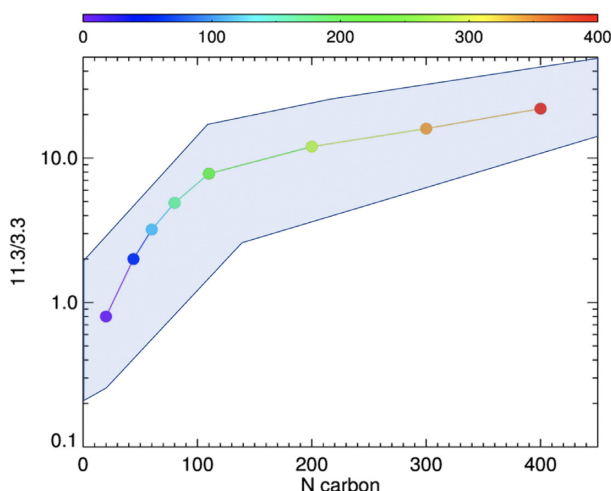
Figure 7. The 11.3/3.3 intensity ratio as a function of N_C for neutral PAHs exposed to the Galaxy ISRF radiation. The shaded region corresponds to the spread of values of each individual PAH considered in this study (see Section 3).

increasing by a factor of ∼10 between small and large N_C values. While the 11.3/3.3 can be used to trace PAH size distribution, it is worth pointing out two factors that can influence the value of this ratio in astronomical sources: the first is the sensitivity of the 3.3 µm band on the hardness of the radiation field. As is shown in Fig. 1, the strength of the 3.3 µm feature is very sensitive to changes in the hardness of the radiation field it is exposed to. In addition, the 11.3/3.3 µm ratio is also affected by extinction as the two features are bound to experience different levels of extinction because of the wavelength difference. In a recent study, Lai et al. (2020) investigated the effect of obscuration on PAH bands and found that among all PAH bands, the 3.3 µm feature is the one that is most susceptible to dust attenuation. In addition, Hernan-Caballero et al. (2020) investigated the effect of extinction on the 11.3 µm feature. While extinction is bound to affect all PAH band ratios, the 6.2/7.7 µm ratio is less susceptible because of the proximity in the wavelengths of the two features. We discuss the dependence of the 11.3/3.3 ratio on the hardness of the radiation field in detail in the next section.

4.2 PAH band ratios versus hardness of the radiation field & charge

The fraction of ionized PAHs at any given time is determined by the balance between photoionization and recombination with ambient electrons. The photoionization is dependent upon the intensity of the radiation field (expressed by G_0, the intensity of the radiation field in units of the solar vicinity value $1.6 \times 10^6\,\mathrm{W\,m^{-2}}$; Habing 1968) whereas the fraction of ambient electrons available for recombination is parameterized by n_e the electron density. Laboratory experiments and theoretical studies (DeFrees et al. 1993; Allamandola et al. 1999; Bakes, Tielens & Bauschlicher 2001) have shown that the ionization of PAHs enhances the intensity of the band features in the 6–9 µm region relative to the features in the 11–14 µm region. Therefore, band ratios involving ionized to neutral bands (such as 6.2/11.3, 7.7/11.3) should provide an estimate of the ionization of PAHs. The PAH *ionization parameter* defined as $G_0 T_{\mathrm{gas}}^{1/2}/n_e$, where T_{gas} is the temperature of the gas in K, can be linked to the fraction of ionized to neutral PAHs and subsequently to PAH band strength ratios. In reality, both G_0 and the fraction of ionized PAHs also depend on the hardness of the underlying radiation field that the PAHs are exposed to.

In order to robustly examine the effect of ionization and of the hardness of the underlying radiation field to PAH band ratios we consider two limiting cases: one with low N_C and one with large N_C molecules. We use the 'bin-averaged' values for PAHs at the low ($20 < N_C < 40$) and high end ($200 < N_C < 400$) of the PAH distribution, as discussed in Section 3 and shown in Fig. 2. In Fig. 8. we examine the dependence of the 11.3/3.3 and 11.3/7.7 band ratios for *small* and *large* PAH molecules on the hardness of the underlying field. The two band ratios were measured when the molecules were exposed to radiation fields of varying strength (from 6 to 12 eV). Both the 11.3/ 3.3 and 11.3/7.7 ratios are sensitive to the strength of the radiation field they are exposed to; however, the 11.3/3.3 ratio shows a much stronger dependence on the hardness of the underlying radiation field. In Fig. Figure 9. we plot the 11.3/3.3 and 11.3/7.7 band ratios for small and large PAH molecules but this time we vary the fraction of neutral-to-ionized molecules, starting from 100 per cent neutral to 100 per cent ionized. We find that the 11.3/7.7 ratio shows a clear dependence on the ionization both for small and large molecules. Hony et al. (2001) studied correlations between PAH bands and mid-IR fine structure lines for a sample of PDRs, H II regions, and molecular clouds in the large magellanic cloud. They found that the ratio of 11.3/7.7 showed only a weak dependence on the [Ne II]/[Ne III] line ratio that they used as an indicator of hardness for the incident radiation field. This result is in line with the finding from our models that indeed the 11.3/7.7 ratio is a good tracer of the ionization fraction of PAH molecules. Mori et al. (2012) suggested that the 11.3/3.3 versus 7.7/11.3 ratio can be used as a diagnostic tool for the radiation field conditions: a harder radiation field will result in increased ionization fraction whereas a softer field will decrease the number of ionized PAH molecules (their figs 6 and 7). In agreement with Mori et al. (2012) we conclude that when combined these two band ratios could be used to probe the physical conditions of the ionizing source.

4.3 The 6.2/7.7 versus 11.3/7.7 and 11.3/7.7 versus 11.3/3.3 ratios

In this section we bring together the results of the analysis described above as we seek to use the various PAH emission bands to construct a size-ionization-hardness grid. The well-established correlation between 6.2/7.7 and N_C, the steep dependence of the 11.3/7.7 on

the fraction of neutral versus ionized molecules, and finally, the ability of the 11.3/3.3 ratio to track the strength of the underlying radiation field *define a three-dimensional plane that can qualitatively characterize the properties of PAHs and infer the conditions of the ISM.* Fig. 10 shows the 3D space defined by combining the three PAH band ratios. The black tracks correspond to neutral PAHs while the magenta dotted line represents the track for ionized PAHs. Fig. 11 shows cuts along the 6.2/7.7 versus 11.3/7.7 and 11.3/3.3 versus 11.3/7.7 planes and these are discussed in the next section.

5 DISCUSSION: COMPARISON BETWEEN MODELS AND DATA

5.1 The sample data

The Infrared Spectrograph (IRS) on board Spitzer and before then the Short Wavelength Spectrometer (SWS) on board *ISO* have acquired mid-IR spectra for a large number of astronomical objects.

Comprising four separate modules, the IRS covered the entire 5.2–38 μm in two resolution modes (Houck et al. 2004). For the present study we focus on the strength of the 6.2, 7.7, and 11.3 PAH lines with values taken from published works on a number of different samples of galaxies including normal, Seyfert, and dwarf galaxies. We only consider PAH band measurements from low resolution spectroscopic observations. The line ratios are plotted against the model grids generated from the synthetic spectra discussed earlier. The galaxies considered here come from the SINGS survey (Smith et al. 2007), the RSA sample of galaxies (Diamond-Stanic & Rieke 2010), and blue compact dwarf galaxies (Hunt et al. 2010). We stress here that we have not made any attempts to re-reduce the spectra in a homogenous manner. A more detailed analysis based on IRS spectral maps will be presented in a future paper García-Bernete et al. (2020).

Fig. 12 shows the 6.2/7.7 versus 11.3/7.7 band ratios for the various galaxy samples outlined above. The tracks shown are for neutral PAHs (black grid) starting from small PAHs ($N_c = 20$) to large
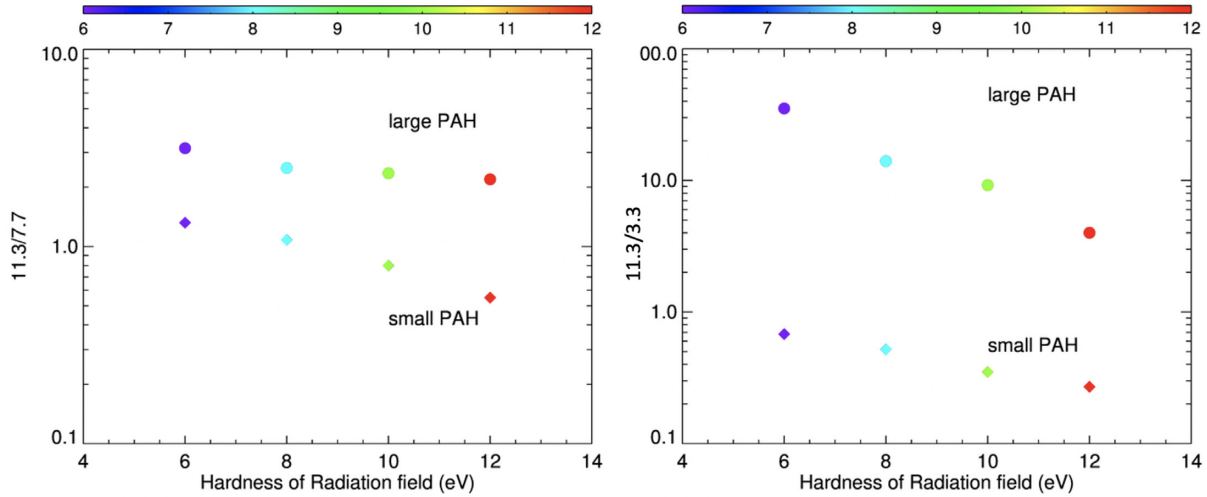

Figure 8. The 11.3/7.7 (left) and 11.3/3.3 (right) intensity ratios calculated for the small bin-averaged molecule (bottom) and the largest bin-averaged (top) neutral PAH molecules as a function of radiation fields with varying energy from 6 to 12 eV. The colour coding corresponds the hardness of the radiation field.
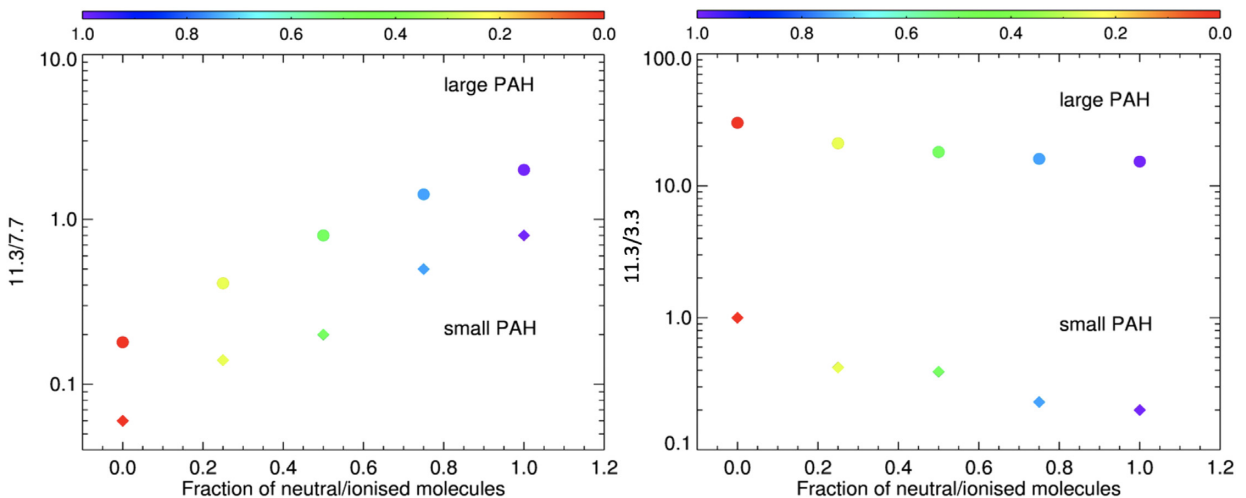

Figure 9. The 11.3/7.7 (left) and the 11.3/3.3 (right) intensity ratios calculated for the small bin-averaged (bottom) and the large bin-averaged (top) PAH molecules with varying degrees of ionization starting from a neutral PAH (0 per cent) to a cation PAH (100 per cent). The colour coding corresponds to fraction of neutral versus ionized molecules.
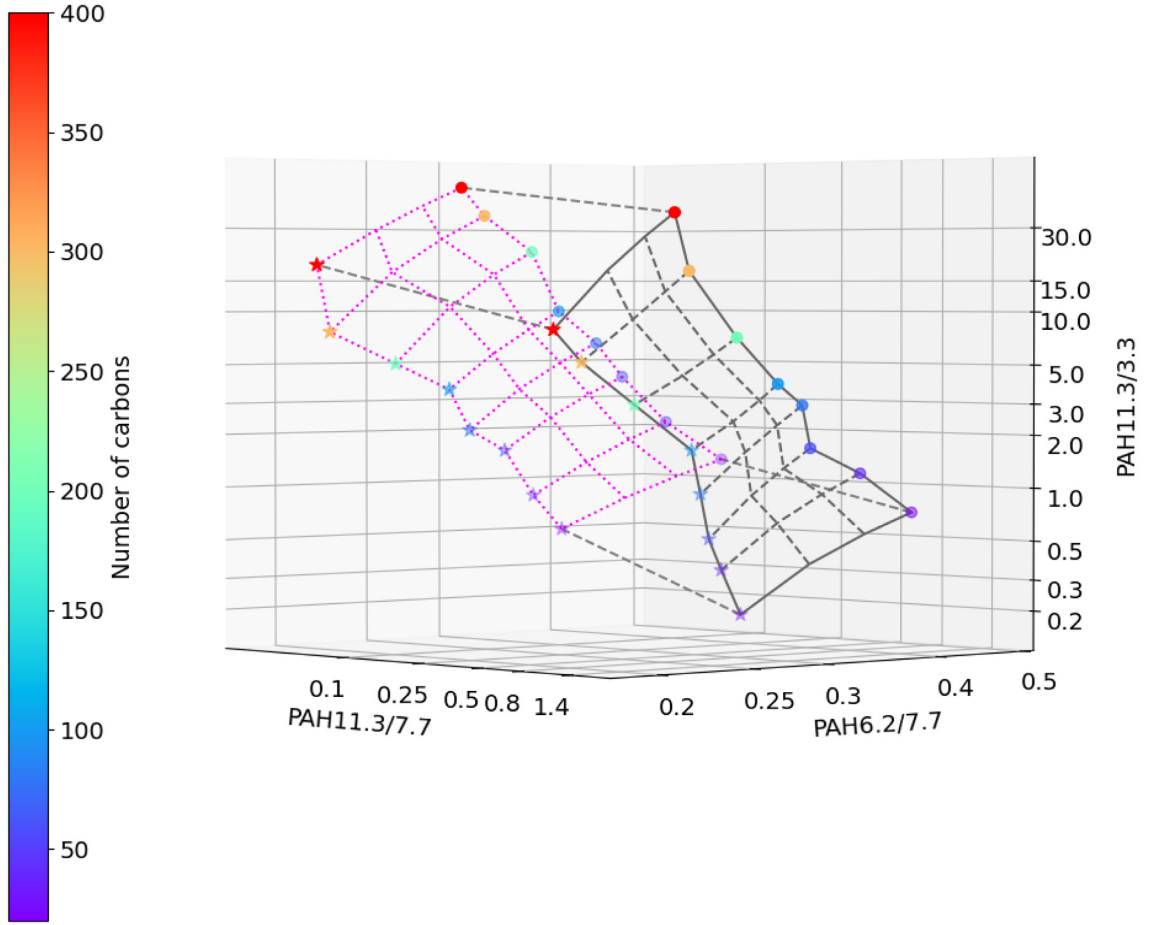
Figure 10. The 3D space defined by the 11.3/3.3 versus 11.3/7.7 versus 6.2/7.7 ratios. The different colours correspond to different number of carbons. The filled circles corresponds to PAHs exposed to ISRF while the filled stars corresponds to $1000 \times$ ISRF. The black tracks correspond to neutral PAHs while the magenta dotted lines corresponds to ionized PAHs.
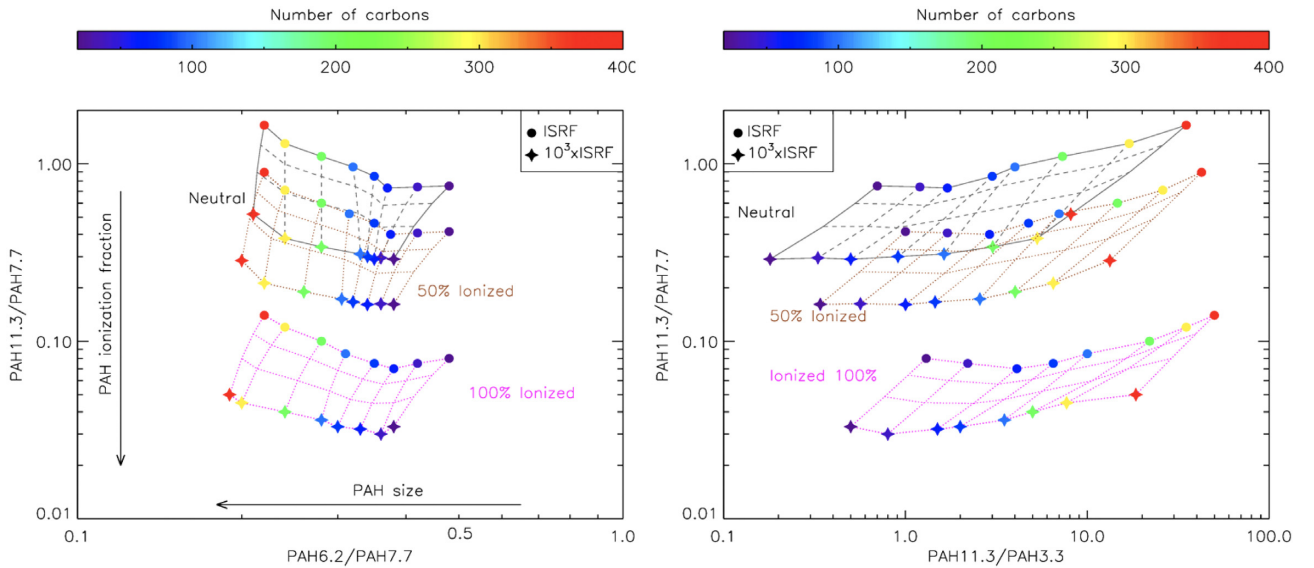
Figure 11. (Left) The 6.2/7.7 versus 11.3/7.7 ratio plot from DFT PAH spectra exposed to radiation fields with a range of energies from the ISRF (filled circles) to $10^3 \times$ ISRF (stars). The top grid (black lines) represents neutral PAHs, the middle grid (brown lines) represents 50 per cent neutral and 50 per cent ionized PAHs while the bottom one (magenta lines) corresponds to 100 per cent ionized PAHs. (Right) The same grids for the 11.3/7.7 versus 11.3/7.7 ratio plot from DFT PAH spectra exposed to radiation fields with a range of energies from ISRF to $10^3 \times$ ISRF.
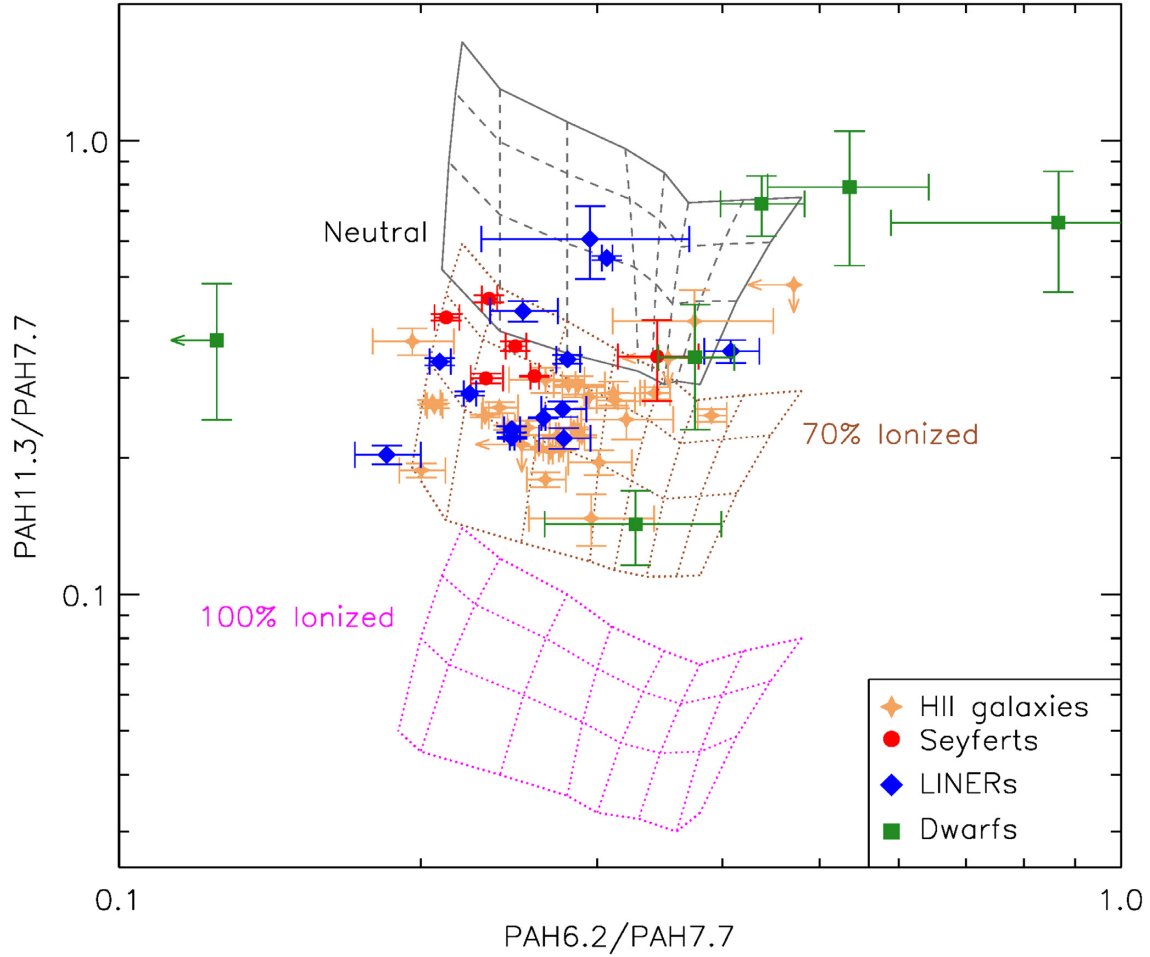
Figure 12. The size-ionization grid (same as in Fig. 10) showing PAH band ratios for normal (H II) galaxies (orange stars), LINERS (blue diamonds), Seyferts (red circles), and dwarf galaxies (green squares). The top grid corresponds to neutral PAHs, the middle grid corresponds to a mixture of 70 per cent ionized–100 per cent neutral, and the bottom one corresponds to the fully ionized PAH grid.

PAHs ($N_c = 400$) and exposed to a radiation field ranging from ISRF to $10^3 \times$ ISRF as discussed in Section 3. In addition we show the track for ionized PAHs (we only show the ISRF case for the ionized PAHs to maintain a clear view of the location of the majority of the galaxies on the plot).

The majority of galaxies seem to preferentially lie at the location of large PAHs with no noticeable difference between the location of LINERS and AGN. H II galaxies appear to favour slightly smaller PAH molecules although with the current data it is difficult to fully quantify the differences. Dwarf galaxies display a wide range of band ratios with roughly half of the sample galaxies falling outside the range covered by the current grid. Likewise, a small fraction of the LINERS also appear to fall outside the grid. While a full discussion of why such sources may be located outside the grid will appear in a forthcoming paper (García-Bernete et al. 2020) we note here that it is likely that the harsh ISM conditions often encountered in dwarf galaxies may be responsible for the presence of catacondensed PAH molecules (those exhibiting open and irregular structure). In his recent review Li (2020) suggests that emission spectra from catacondensed molecules have a higher 11.3/7.7 ratio. It is also likely that such extreme 11.3/7.7 ratios could be due to incomplete subtraction of the continuum emission underlying the PAH bands. The higher sensitivity and spectral resolution afforded with the upcoming *James Webb Space Telescope* (*JWST*) is expected to shed light on PAHs

in a variety of extragalactic conditions. It is, however, clear that very few galaxies lie in the location of the grid where $20 < N_C < 50$. In terms of ionization, it is evident that most galaxies require a fraction of ionized PAHs between 25 per cent to 50 per cent with some normal/star-forming galaxies requiring >75 per cent ionized PAH molecules.

6 CONCLUSIONS

Based on DFT-computed PAH spectra we have presented a method to investigate the size, charge, and hardness of the radiation field based on combinations of PAH band ratios. The DFT spectra were computed for molecules with varying number of carbons in the range of $20 < N_C < 400$. The spectra were generated using the Gaussian software and supplemented with spectra from the NASA Ames PAH IR Spectroscopic Database. The spectra were stacked in bins of increasing size and in each bin an 'averaged' spectrum was calculated. 3σ outliers were removed from further analysis. The spectra were subsequently 'exposed' to radiation fields corresponding to multiples of the ISRF, the interstellar radiation field of our Galaxy. We considered neutral as well as cationic molecules. Our findings can be summarized as follows:

(i) PAH sizes: We have explored several band ratios to determine the optimal ones to trace the PAH molecular size. We investigated combinations of PAH band ratios originating from the bending or stretching of C–H or C–C bonds and focus in particular on the 6.2/7.7 and/or 11.3/3.3 ratios. Both ratios can be used to track PAH molecular size. The 6.2/7.7 ratio changes by a factor of 2 between small and large molecules and is less sensitive to interstellar extinction since the wavelengths of the features lie close together. The 11.3/3.3 varies by a factor of 10 between small and large molecules although the ratio is sensitive to extinction [see discussion in Lai et al. (2020) for the 3.3 μm and Hernan-Caballero et al. (2020) for the 11.3 μm]. In addition, this ratio shows a strong dependance on the hardness of the radiation field.

(ii) Hardness of the underlying radiation field: We have explored the influence of the hardness of the underlying radiation field on PAH band ratios. We explored the effects of varying the intensity of the radiation field on two limiting cases, the bin-averaged small and the bin-averaged large PAH molecules. We found that the 11.3/3.3 band ratio shows a good correlation with the intensity of the radiation field with the ratio decreasing with increasing energy. A similar trend is noted by Mori et al. (2012) for their Group A sources.

(iii) Fraction of neutral-to-ionized PAH molecules: We explored ratios sensitive to the fraction of neutral-to-ionized molecules. Amongst the band ratios examined we found that the 11.3/7.7 increases steeply as we progress from 100 per cent neutral to 100 per cent ionized molecules.

(iv) We have compared published Spitzer IRS data from samples of normal, star-forming, dwarf galaxies as well as AGNs to our grids. We find that the majority of galaxies tend to favour large PAHs exposed to radiation fields of moderate strength. The majority of the sample galaxies favour an ionization (fraction of neutral to ionized molecules) of <1 with the star-forming galaxies requiring a higher fraction of charged PAHs. It is obvious from Fig. 12 that we need to investigate the behaviour of large molecules with $N_C >$ 500 as the majority of the band ratios seen in galaxies tend to favour large molecules. This issue will be addressed in a forthcoming paper (Kerkeni et al., in preparation).

(v) We have demonstrated that by combining the three ratios 6.2/7.7, 11.3/3.3, and 11.3/7.7, we can qualitatively constraint the size and the physical conditions in the regions where PAHs originate. The upcoming availability of *JWST* will enable measurements of these bands in a number of galactic and extragalactic sources. In addition, we will be able to study these ratios within regions of galaxies and map out the influence of the underlying radiation source (star or AGN) on the immediate surroundings and explore the fate of small/large PAHs.

ACKNOWLEDGEMENTS

DATA AVAILABILITY

The data underlying this article will be shared on reasonable request to the corresponding author.

REFERENCES

Allamandola L. J., Hudgins D. M., Sandford S. A., 1999, ApJ, 511, L115
Allamandola L. J., Tielens A. G. G. M., Barker J. R., 1989, ApJS, 71, 733
Alonso-Herrero A. et al., 2014, MNRAS, 443, 2766
Alonso-Herrero A. et al., 2016, MNRAS, 463, 2405
Bakes E. L. O., Tielens A. G. G. M., 1994, ApJ, 427, 822
Bakes E. L. O., Tielens A. G. G. M., Bauschlicher C. W., 2001, ApJ, 556, 501
Bauschlicher C. W., 2002, ApJ, 564, 782
Bauschlicher C. W., Ricca A., Boersma C., 2018, ApJS, 234, 32
Blommaert J. A. D. L., Cami J., Szczerba R., Barlow, M. J., 2005, Space Science Reviews, 119, 215
Boersma C., Bregman J. D., Allamandola L. J., 2013, ApJ, 769, 117
Boersma C. et al., 2014, ApJS, 211, 8
Boulanger F., Boissel P., Cesarsky D., Ryter C., 1998, A&A, 339, 194
Brandl B. R. et al., 2006, ApJ, 653, 1129
Bregman J., Temi P., 2005, ApJ, 621, 831
Croiset B. A., Candian A., Berne O., Tielens A. G. G. M., 2016, A&A, 590, 26
DeFrees D. J., Miller M. D., Talbi D., Pauzat F., Ellinger Y., 1993, ApJ, 408, 530
Desai V., et al., 2007, ApJ, 559, 810
Diamond Stanic A. M., Rieke G. H., 2010, ApJ, 724, 140
Draine B. T., Li A., 2001, ApJ, 551, 807
Draine B. T., Li A., 2007, ApJ, 657, 810
Engelbracht C. W.,, Rieke G. H., Gordon K. D., Smith J.-D. T., Werner M. W., Moustakas J., Willmer C. N. A., Vanzi L., 2008, ApJ, 678, 804
Frisch M. J., et al., 2009, Gaussian 09. Gaussian, Inc., Wallingford, CT
Galliano F., Madden S. C., Tielens A. G. G. M., Peeters E., Jones A. P., 2008, ApJ, 679, 310
González-Martín O., et al., 2013, A&A, 553, 35
Habing H. J., 1968, Bull. Astron. Inst. Netherlands, 19, 421
Hernan-Caballero A. et al., 2020, MNRAS, 497, 4614
Hollenbach D., Tielens A. G. G. M., 1997, ARA&A, 35, 179
Hönig S., Kishimoto M., Gandhi P., Smette A., Asmus D., Duschl W., Polletta M., Weigelt G., 2010, A&A, 515, 23
Hony S., Van Kerckhoven C., Peeters E., Tielens A. G. G. M., Hudgins D. M., Allamandola L. J., 2001, A&A, 370, 1030
Houck J. R. et al., 2004, ApJ, 154, 18
Huang J.-S. et al., 2007, ApJ, 660, L69
Hudgins D. M., Allamandola L. J., 2001, A&A, 370, 1030
Hunt L. K., Thuan T. X., Izotov Y. I., Sauvage M., 2010, ApJ, 712, 164
Jensen J. J., et al., 2017, MNRAS, 470, 3071
Joblin C., Leger A., Martin P., 1992, ApJ, 393, L79
Jourdain de Muizon M., D' Hendecourt L. B., Geballe T., 1990, A&A, 227, 526
Kessler M. F., et al., 1996, A&A, 315, 27
Kim H.-S., Saykally R. J., 2002, ApJS, 143, 455
Lai T. S.-Y., Smith J. D. T., Baba S., Spoon H. W. W., Imanishi M., 2020, ApJ, 905, 55
Langhoff S., Bauschlicher C. W., 1994, LNP, 248, 310
Leger, Puget, 1984, A&A, 137, 5
Leger A., d'Hendecourt L., Defourneau D., 1989, A&A, 216, 148
Li A., 2020, Nat. Astron., 4, 339
Malloci G., Joblin C., Mulas G., 2007, A&A, 462, 627
Maragkoudakis A., Peeters E., Ricca A., 2020, MNRAS, 494, 642
Mattioda A. L., Allamandola L. J., Hudgins D. M., 2005, ApJ, 629, 1183
Mattioda A. L. et al., 2005, ApJS, 251, 22
Mori T. I., et al., 2012, ApJ, 744, 68
Moutou C., Sellgren K., Leger A., Verstraete L., Rouan D., Giard M., Werner M. 1998, in Yun J., Liseau L., eds, ASP Conf. Ser. Vol. 132,

Star Formation with the Infrared Space Observatory. ASP, San Francisco, CA, p. 47

Peeters E., Bauschlicher C.W., Jr., Allamandola L. J., Tielens A. G. G. M., Ricca A., Wolfire M. G., 2017, ApJ, 386, 198

Peeters E., Spoon H. W. W., Tielens A. G. G. M., 2004, ApJ, 613, 986

García-Bernete I., Rigopoulou D., Alonso-Herrero A., Pereira-Santaella M., Roche P. F., Kerneki B., 2020, preprint (arXiv:2011.10882)

Pope A., et al., 2013, ApJ, 772, 92

Ricca A., Bauschlicher C. W., Jr., Boersma C., Tielens A. G. G. M., Allamandola L. J., 2012, ApJ, 754, 75

Ricca A., Bauschlicher C. W., Jr., Roser J. E., Peeters E., 2018, ApJ, 854, 115

Riechers D., et al., 2014, ApJ, 796, 84

Rigopoulou D., Spoon H. W. W., Genzel R., Lutz D., Moorwood A. F. M., Tran Q. D., 1999, AJ, 118, 2625

Roche P. F., Aitken D. K., Smith C. H., 1989, MNRAS, 236, 485

Sales D. A., Pastoriza M. G., Riffel R., 2010, ApJ, 725, 605

Schutte W. A., Tielens A. G. G. M., Allamandola L. J., 1993, ApJ, 415, 397

Shipley H. V., Papovich C., Rieke G. H., Brown M. J. I., Moustakas J., 2016, ApJ, 818, 60

Sloan G. C. et al., 2007, ApJ, 664, 1144

Smith J. D. T., et al., 2007, ApJ, 656, 770

Stock J. D., Peeters E., 2017, ApJ, 837, 129

Sturm E., Lutz D., Tran D., Feuchtgruber H., Genzel R., Kunze D., Moorwood A. F. M., Thornley M. D., 2000, A&A, 358, 481

Tielens A. G. G. M., 2008, ARA&A, 46, 289

Tran Q. D., et al., 2001, ApJ, 552, 527

VastelC., Caux E., Glorian J.-M., Boiziot M., 2015, in F. Martins, S. Boissier, V. Buat, L. Cambresy, P. Petit , eds. SF2A-2015: Proceedings of the Annual meeting of the French Society of Astronomy and Astrophysics . , p. 313.

Venables W. N., RipleyB. D., 2002, Mod. Appl. Stat. S, 271, 300

Verstraete L., et al., 2001, A&A, 372, 981

Werner M., et al., 2004, ApJS, 154, 1

APPENDIX A: PAH MOLECULES

Table A1 lists all the molecules used in this study. The numbers reported correspond to the UIDs in the NASA Ames Database for neutral and cationic molecules. Where there is no UID entry, the frequencies of those molecules have been computed by us. A discussion of the methodology followed to compute the vibrational spectra of various PAH molecules will appear in Kerkeni et al. (in preparation) as described in Section 2.

Table A1. Molecules used in this study.

Molecule	Neutral	Cation	Molecule	Neutral	Cation
C22H12	2347	3156	C22H14	301, 305, 307	302, 306, 308
C24H12[1]			C27H13	66	65
C30H14[1]			C31H15	3226	3227
C32H14[1]			C34H16	3161	3162
C35H15	3229	3230	C36H16[1]		
C37H15	3232	3234	C40H18	131, 533, 625	132, 540, 626
C42H18[1]			C42H22	137, 156	138,158
C43H17	3235	3236	C44H18[1]		
C44H20	140	141	C45H15	718	722
C45H17	3238	3239	C46H18	3169	3170
C47H17	76	77	C48H18[1]		
C48H20	100, 146	101, 147	C48H22	143, 3941, 3942, 3943	144, 3957, 3958, 3959
C51H19	3241	3242	C52H18	3173	3174
C54H18[1]			C54H20	3176	3177
C55H19	3244	3245	C56H20	3179	3180
C57H19	646	644	C58H20[1]		
C59H21	3247	3248	C62H20[1]		
C63H21	727	730	C64H20	3188	3189
C64H22	3191	3192	C65H20[1]		
C66H18	713, 714	715, 716	C66H20[1]		
C67H21	656	654	C67H23	3252, 3255	3253, 3256
C71H21	659	657	C72H22	3194	3195
C73H21	3257	32578	C76H22	3197	3198
C77H23	3260	3261	C78H22[1]		
C82H24	561, 3203	562, 3204	C83H23	3265	3266
C85H23	3268	3269	C87H23	649	647
C88H24[1]			C90H24	638	639
C91H25	3273	3274	C94H24	3211	3212
C95H25	3277	3278	C95H27	3280	3281
C96H23	693, 696	694, 697	C96H24[1]		
C98H28	565, 567	566, 568	C102H26	177, 180, 3214	178, 181, 3215
C103H27	3285	3286	C107H27	3287, 3289	3288, 3290
C108H26	3217	3218	C110H26	162	163
C111H27	3291	3292	C112H26[1]		
C115H29	3296	3297	C128H28	631	632
C130H28	168	169	C138H30	772	773
C142H30	760, 763, 766	761,764, 767	C144H30	756, 641	757, 642
C146H30	746, 749, 752	747, 750, 753	C148H30	743	744
C150H30	612	613	C170H32	619	623
C190H34	634	738	C210H36	742	740
C294H42	616		C384H48[1]	617	

[1]Vibrational frequencies for these molecules have been computed independently.

APPENDIX B: IONIZED PAHS

In addition to the neutral PAHs we have followed the same procedure to compute DFT-spectra for PAH cations (corresponding to the neutral PAHs used in our study). To compute the spectra of the cations we followed the same steps as outlined in Section 2, using the same B3LYP functional along with the 4-31G basis set. The DFT-computed transition frequencies for the PAH cations were subsequently convolved with a specific band shape, line width, and emission temperature to convert them to emission spectra. Applying the same methodology as with the neutral PAH spectra, we placed the cation spectra in bins (see Fig. 2) and for each bin we computed an average spectrum by determining the arithmetic mean and dividing the average value by the number of molecules that were assigned to that bin. Fig. A1 shows the relative intensities of the 3.3, 6.2, 7.7, 8.6, 11.3 μm cation PAH emission bands calculated based on the ISRF emission model. The figure shows the average intensities as well as the 3σ spread around this value for every bin.
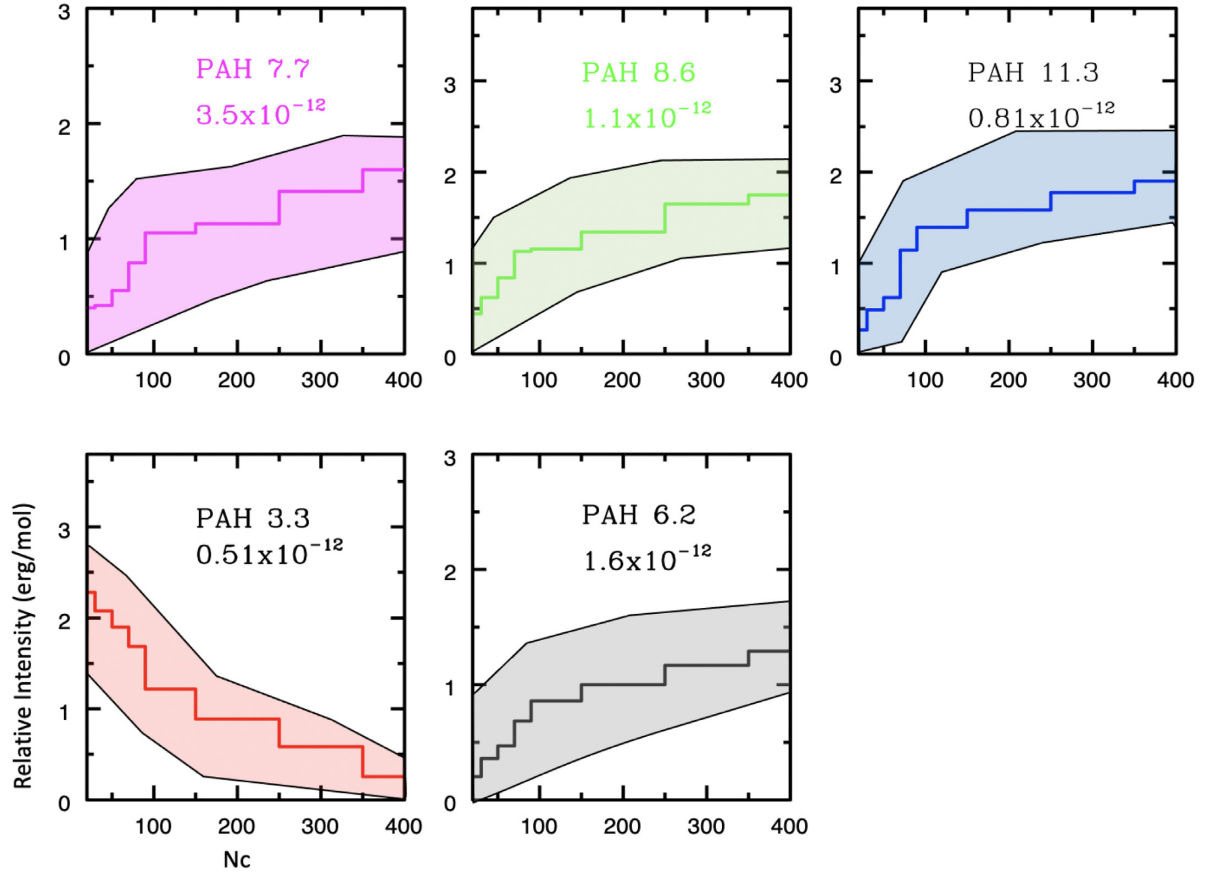
Figure B1. Intensities for cationic PAHs (3.3, 6.2, 7.7, 8.6, and 11.3 μm) as a function of N_C, with normalizations shown in each panel. The average value in each bin is denoted with the line while the shaded regions denote the spread of values in each bin. PAHs with intensity values greater than 3σ have been excluded. The plots are normalized to N. The intensities have been calculated for the ISRF radiation field. Colour coding: 3.3 μm (red), 6.2 μm (grey), 7.7 μm (magenta), 8.6 μm (green), 11.3 μm (blue).

This paper has been typeset from a TEX/LATEX file prepared by the author.